POLITECNICO DI TORINO
Repository ISTITUZIONALE

A multibody simulation of a human fall: Model creation and validation

(Article begins on next page)

26 April 2024

AIAS 2019 International Conference on Stress Analysis

A multibody simulation of a human fall: model creation and validation

Giulia Pascoletti[a], Daniele Catelani[b], Paolo Conti[a], Filippo Cianetti[a], Elisabetta M. Zanetti[a][*]

[a]University of Perugia – Departement of Engineering, Via G. Duranti 93, Perugia 06125, Italy
[b]MSC Software Corporation, Via Santa Teresa 12, Torino 10121, Italy

Abstract

This work is focused on the analysis of the fall of a human being from a given height. With reference to forensic disputes, the final subject position is often the only evidence and foreseeing the body trajectory and the respective driving force may not be trivial. This article illustrates how multibody models can be used for this aim.

A multibody model of a human subject has been built, given his stature and his known mass. This model was made of 15 segments, whose inertial properties, joint centres and volumes were deduced from anthropometric databases. This model was validated against experimental tests performed on a Hybrid III dummy: it was able to reproduce the peak impact head force with an error lower than about 10%.

Some examples are produced to illustrate the usefulness of this validated model as a tool for the analysis of falls, and how it can be easily parametrized to make multiple simulations with different initial conditions/environment configurations. As such it is a valuable tool for forensic analyses

Keywords: Fall from height; multibody model; anthropometric data; forensic biomechancis

[*] Corresponding author. Tel.: +39 075 5853704; fax: +39 075 5853704.
E-mail address: Elisabetta.zanetti@unipg.it

10.1016/j.prostr.2020.02.031

1. Introduction

Fall from height represents one of the main causes of occupational fatalities: they account for 42% of fatalities in construction industry according to NIOSH (National Institute for Occupational Safety and Health) (Dong et al., (2017)). A high incidence is also reported from a smaller database pertaining Piedmont Italian region where these falls account for 41% fatalities (Farina et al., (2019)). Discriminating among accidental, self-inflicted accidents or assaults might not be trivial. As a matter of fact, the only experimental evidences are body injuries and the final body position. Forensic medicine is producing continuous efforts to give some clues about the fall causes and modalities, based on injuries examination (Atanasijevic et al., (2015); Rowbotham et al., (2018); Rowbotham et al., (2016)). Biomechanics can give a contribution as well, through dynamic analyses (Muggenthaler et al., (2013)). It is a sort of backward problem where, given the final position, the input force and the initial position are to be determined. This kind of analyses can be performed experimentally or numerically. Experimentation cannot be exhaustive for various reasons: the dummy model will never be identical to the victim, therefore some sort of generalization is required. Secondly, the number of measured quantities is usually quite limited, therefore analytic calculations are required to derive further information. Finally, the number of tests which can be performed is usually restricted, while backwards analyses often require testing many combinations of input parameters: the initial body position, muscles activation level, eventual applied forces. Nonetheless, experimentation remains a mandatory step since whatever numerical model needs to be validated in order to provide reliable results. As well known, numerical simulations always come from a simplified model, and experimental results allow assessing deviations from reality that is the impact of simplifications on results.

The simplest human models are made of solid bodies, joined at the locations of their skeletal articulations. These models are adequate to forecast the overall kinematic behavior of the human body, or to provide input forces/displacements for detailed analyses of deformable organs which are usually performed by finite element codes. A further evolution is making use of multibody models including some flexible bodies (Pascoletti et al., (2018); Putame et al., (2019); Terzini et al., (2017); Zanetti et al., (2017), (2018)) which represents components undergoing large deformations.

A question which needs to be specifically addressed is the contribute given by muscles during motion. In facts, both passive and active models are available (Milanowicz et al., (2017)). The use of active models is generally discouraged since, with few exceptions, it is impossible to know muscle activation patterns versus time, and they can't either be calculated from kinematics. In facts, this problem (that is the so-called 'inverse dynamic problem' of neuro-muscular system) is ill-posed since many different activation patterns are able to produce a given trajectory. The consequence is that only phenomena where muscle activation is irrelevant can be properly modelled or situations where muscle activation is quite predictable, responding to unconditional reflexes.

Generally, passive models are used as a first approach since active models would include a very high number of variables whose value is unknown. Some active elements (muscles) are introduced in the following step, based on discrepancies between the passive model results and the actual final position of the injured human being. Many passive multibody models have been developed in literature, however complete details about joint stiffness and contact parameters have been seldom reported in a systematic way, making hard a comparison among the respective results or the construction of similar models for the analysis of other events; this work gives a contribute in this sense, explicating all these data.

2. Materials and methods

2.1. Geometry model

The human body model is an articulated total body android made of 15 elements and 14 joints between them. Each element is an ellipsoid with a center of mass (CM) coordinate system, proximal and distal coordinates systems, with assigned mass and inertial properties. The latter properties have been derived from the fiftieth percentile, according to UMTRI reports (Robbins, (1983)). The correspondence between each segment and the respective human body part is described in Fig. 1 and Table 1.
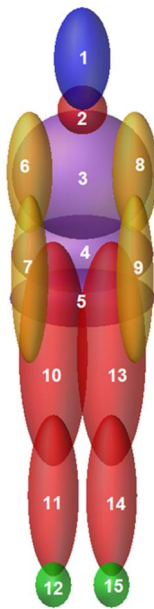
Fig. 1. Articulated Total Body segments.

Table 1. Segments name and location.

Segment Number	Segment Name
1	Head
2	Neck
3	Upper Torso
4	Central Torso
5	Lower Torso
6	Right Upper Arm
7	Right Lower Arm
8	Left Upper Arm
9	Left Lower Arm
10	Right Upper Leg
11	Right Lower Leg
12	Right Foot
13	Left Upper Leg
14	Left Lower Leg
15	Left foot

The following figure shows geometries corresponding to upper and lower arm (*i* segment and *j* segment respectively) and the associated coordinates systems.
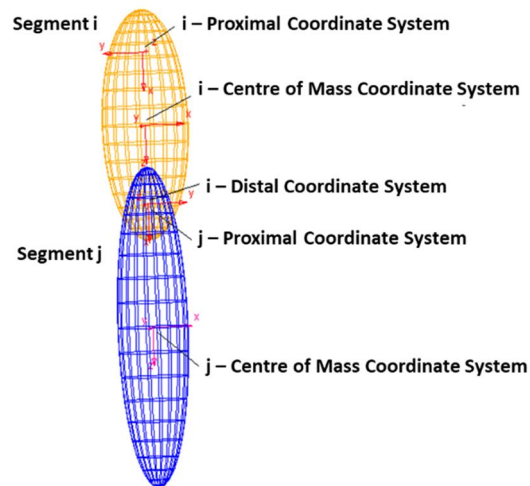
Fig. 2. Principal coordinates systems of ellipsoids.

The proximal and the distal coordinate systems are the reference marker for the connection joint between two adjacent segments; in fact, each constraint requires the creation of two markers with the same location and orientation. Therefore, with reference to Fig. 2, the *i* distal coordinate system and the *j* proximal coordinate system define the location and orientation of the connection joint between the upper arm and the lower arm, that is the elbow joint.

2.2. Connection joints

The actual human joints have been modelled with classical mechanical connection joints or with combinations of these, in order to approximate as faithfully as possible, the degrees of freedom of each joint in the human body.

Table 2. Human joint modelling.

Human Joint	Connection Joint	DOF
Upper Neck	Spherical	3 Rotations
Lower Neck	Spherical	3 Rotations
Right/Left Shoulder	Spherical with Perpendicular	2 Rotations (rotation along the long axis segment is removed)
Right/Left Elbow	Revolute	1 Rotation in the sagittal plane
Lumbar Spine	Spherical	3 Rotations
Thoracic Spine	Spherical	3 Rotations
Right/Left Hip	Spherical with Perpendicular	2 Rotations (rotation along the long axis segment is removed)
Right/Left Knee	Revolute	1 Rotation in the sagittal plane
Right/Left Ankle	Revolute	1 Rotation in the sagittal plane

Table 2 reports in detail the degrees of freedom of each joint; some joints have been 'simplified' (the shoulder joint for example) having considered that the final aim of this work was to properly simulate the fall from height of a human being and some degrees of freedom were not so relevant in relation to this aim. This is the reason why no axial rotation along long bone axes have been considered, as well as abduction/adduction movements of elbows, knees and ankles.

For right and left spherical joints, reference coordinates systems have been oriented as depicted, as example, in Fig. 3 for shoulder's joints. Joint's reference coordinates systems are symmetrical with respect to sagittal plane, so that positive and negative rotations around x and y axes represent the same motion for both sides, while rotation along z axis have opposite signs for the same movement.
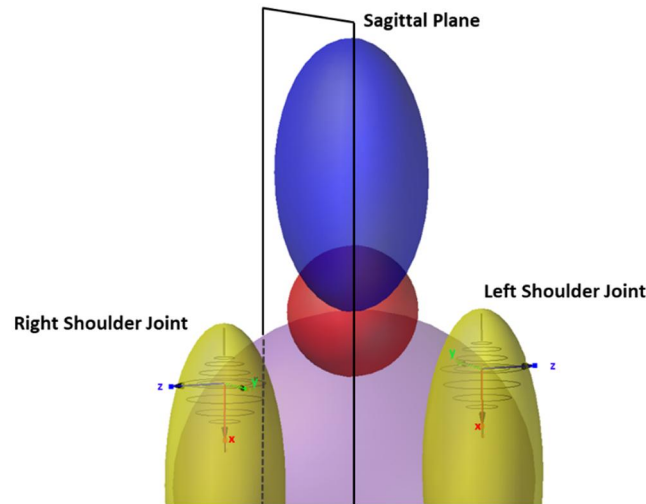
Fig. 3. Joint's reference coordinates system for the left and right shoulders.

2.3. Joints passive resistive torques

One of the major issues when modeling the articulated total body is the identification of the passive resistance of each joint (torque/rotation functions). These resistances act against joint movements and they have been modelled as non-linear springs between two adjacent segments.

These moments have the dual role of:

- Limiting the range of motion of the joint during movements
- Preventing the segments collapsing under their own weight.

A detailed literature research of rotational stiffness characteristics has been performed (Bergmark, (1989); Engin, (1979); Engin et al., (1987); Haug et al., (2004); Riener et al., (1999); Sharan et al., (2013)). For some joints, a non-linear resistive torque law as a function of the segment's motion angles, has been implemented, while for other movements a rotational stiffness value has been provided.   Table 3 shows the resistive moment law or the stiffness value for each joint's degree of freedom, as implemented in this work. The same table reports also the range of motion for each degree of freedom.

Table 3. Rotational resistive characteristics of connection joints.

Human Joint	Joint Movement	Resistive Moment [Nm]	Stiffness Value [Nm/°]	Range of Motion (ROM)
Upper/Lower Neck (Haug et al., (2004))	Flexion		1.4	0° - 60° [0° - 20°]
	Extension		2.5	0° - 75° [0° - 10°]
	Lateral Bending		2.2	0° - 45°
	Twist		0.5	0° - 50°
Shoulder (Engin, (1979))	Flexion/Extension	$e^{(3.3671*(-\theta_S-0.2543))} + -e^{(-3.5743*(-2.1966+\theta_S))}$		-50° - 180°
	Abduction/Adduction	$0.77 - 9.21\theta_s + 4.99\theta_s{}^2 + 5.46\theta_s{}^3 + +0.86\theta_s{}^4 - 10.12\theta_s{}^5 + 6.42\theta_s{}^6 +$		-50° - 160°

		$-1.18\theta_s{}^7$	
	Abduction in Frontal Plane	$-592.67 + 1766.31\theta_s - 2070.46\theta_s{}^2 +$ $+1190.19\theta_s{}^3 - 335.65\theta_s{}^4 + 37.28\theta_s{}^5$	0° - 160°
Thoracic (Sharan et al., (2013))	Flexion	3	0° - 50° [0° - 10°]
	Extension	3.4	0° - 45° [0° - 5°]
	Lateral Bending	2	0° - 40° [0° - 20°]
	Twist	2.5	0° - 30°
Lumbar (Bergmark, (1989); Sharan et al., (2013))	Flexion	1.8	0° - 90° [0° - 45°]
	Extension	2.5	0° - 20° [0° - 10°]
	Lateral Bending	1.3	0° - 35° [0° - 20°]
	Twist	6.9	0° - 20°
Elbow (Engin and Chen, (1987))	Flexion	$e^{(8.7084*(-\theta_E+0.1201))} +$ $-e^{(9.4336*(-2.3187+\theta_E))}$	0° - 150°
Hip (Haug et al., (2004); Riener and Edrich, (1999))	Flexion/Extension	$e^{(1.4655-(0.0034\theta_K-0.075\theta_H))} +$ $-e^{(1.3403-0.0226\theta_K+0.0305\theta_H))} + 8.072$	-30° - 150° [-30° - 50°]
	Abduction in the Frontal Plane	1.2	0° - 80°
	Adduction in the Frontal Plane	0.8	0° - 30°
Knee (Riener and Edrich, (1999))	Flexion	$e^{(1.8-0.0460*\theta_A-0.0352*\theta_K+0.0217*\theta_H)} +$ $- e^{(-3.971-0.0004*\theta_A+0.0495*\theta_K-0.0128*\theta_H)} +$ $-4.820 + e^{(2.220-0.150*\theta_K)}$	0° - 150°
Ankle (Haug et al., (2004))	Plantar flexion	0.3	0° - 50°
	Dorsiflexion	0.5	0° - 30°

Flexion and extension movements of arms and legs have been widely investigated in literature (Engin, (1979); Prasad et al., (2010); Riener et al., (1999)) and for this reason many different angular laws are available. These experimental laws have been analyzed and compared in order to establish which trend was the most reliable, having found the largest consensus among authors.

Whenever joint resistance has been implemented with a spline, similar trends have been adopted. As an example, in Fig. 4a the shoulder flexion/extension curve is shown.
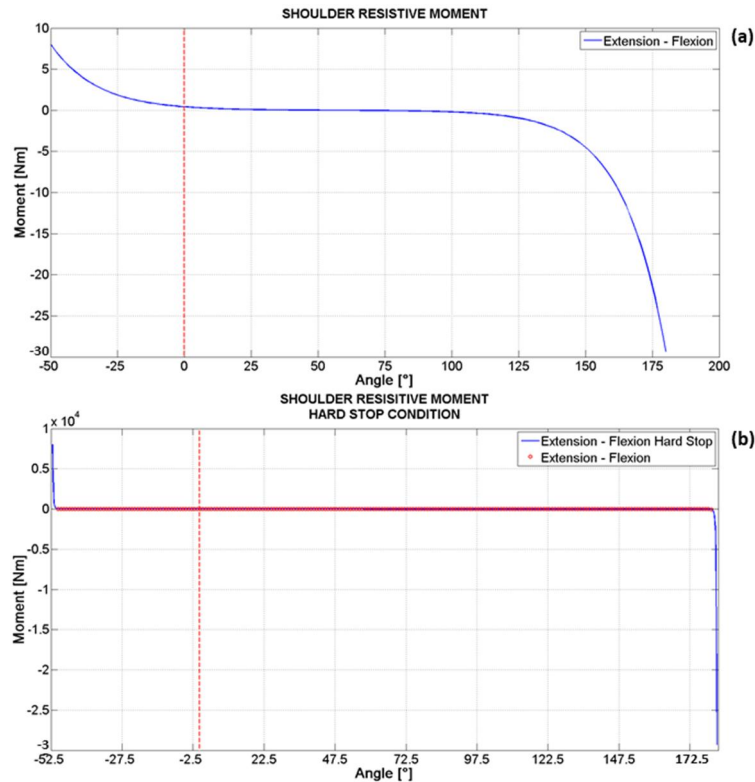
Fig. 4. (a) Shoulder flexion/extension resistive moment; (b) Modified resistive moment.

The zero-angle condition of all joints has been defined with reference to the straight standing position (Fig. 1); starting from this value, there is a range of angles, within the joint's ROM, where the resistive torque is very low (near to zero). On the other side, when the joint's rotation is close to the extreme of the ROM, the resistive torque increases sharply.

These stiffness laws have been modified in order to comply with the range of motion of each joint, adding a 'hard stop' condition (Fig. 4b). According to this condition, when an extreme rotation is approached, the torque value increases, within a motion of 2°, up to 1000 times the value it had in correspondence of the limit. In this way the final spline appears as the one reported in Fig. 4b and ensures that a high resistive torque is applied and no further rotations are allowed.

For the same reason also the linear stiffness characteristics have been modified so that, once a ROM limit is reached, the rotational stiffness rises up to 10000 Nm/° within 2° rotation.

In addition, all the resistive characteristics have been integrated with a constant viscous damping component. Damping coefficients were retrieved from literature (Cheng et al., (1998)) (Table 4) and their main effect is reducing unrealistic vibrations.

Table 4. Damping coefficients for each joint.

Human Joint	Joint Movement	Viscous Damping Coefficient [Ns/m]
Upper/Lower Neck	Flexion Extension Lateral Bending Twist	0.0678
Shoulder	Flexion/Extension Abduction/Adduction Abduction in Frontal Plane	0.0678
Thoracic	Flexion Extension Lateral Bending Twist	0.0565
Lumbar	Flexion Extension Lateral Bending Twist	0.0565
Elbow	Flexion	0.0339
Hip	Flexion/Extension Abduction in the Frontal Plane Adduction in the Frontal Plane	0.0339
Knee	Flexion	0.0339
Ankle	Plantar flexion Dorsiflexion	0.0339

2.4. Model contacts

Contact forces have been implemented for lower limb and upper limb geometries. These contacts are designed to avoid unrealistic segment's compenetration.

Contact stiffness was assigned 'soft' values, having considered the skin effect and having verified it was sufficient to avoid large compenetration.

Table 5 shows the implemented contacts and contact's parameters required for the definition of the force as detailed in the following equation.

$$F_n = K \cdot g^e + STEP(g, 0, d_{max}, C_{max}) \cdot \frac{dg}{dt} \tag{1}$$

where g is the penetration between geometries, dg/dt is the penetration velocity, e is the elastic force component, d_{max} is the penetration depth value for the application of the damping coefficient C_{max}.

Table 5. Contacts.

Contact	Contact Parameters
I geometry: Right Upper Leg - J geometry: Left Upper Leg	
I geometry: Right Lower Leg - J geometry: Left Lower Leg	
I geometry: Right Upper Arm - J geometry: Left Upper Arm	
I geometry: Right Lower Arm - J geometry: Left Lower Arm	
I geometry: Right Upper Arm - J geometry: Left Lower Arm	
I geometry: Right Lower Arm - J geometry: Left Upper Arm	$K = 1 \times 10^3\ N/m^e$
I geometry: Left Upper Arm - J geometry: Head	$e = 1.1$
I geometry: Right Upper Arm - J geometry: Head	$C_{max} = 1 \times 10^4\ Ns/m$
I geometry: Left Lower Arm - J geometry: Head	$d_{max} = 1 \times 10^{-4}\ m$
I geometry: Right Lower Arm - J geometry: Head	
I geometry: Left Upper Arm - J geometry: Upper Torso	
I geometry: Right Upper Arm - J geometry: Upper Torso	
I geometry: Left Upper Arm - J geometry: Central Torso	
I geometry: Right Upper Arm - J geometry: Central Torso	

The model can be easily parametrized for different initial conditions (initial position, speed, eventual applied forces) and allows testing many different combinations of parameters.

3. Results

As a first step, the model has been statically validated.

In order to obtain a statically determined model, joint's torque implemented with spline have been 'compensated', as detailed in the following. Joint resistance curves were derived from experimental laws, therefore resistive torques may deviate slightly from a null value in correspondence of the zero angle of rotation; this value was subtracted from the full curve, resulting in a vertical translation which forces the curve to pass by the axes origin. This procedure ensures that the starting position, that is the straight standing configuration, is in equilibrium.

The model has been dynamically validated comparing results of simulations with experimental results performed by Hajiaghamemar et al., (2015) with a Hybrid III anthropomorphic dummy. In this study five simple scenarios of a fall have been tested and head impact parameters have been calculated. These same configurations have been simulated with the developed model (Fig. 5) and results have been compared (Table 6). With reference to scenario 5, the left upper arm has been deactivated in order to reproduce the experimental setup (Hajiaghamemar et al., (2015)) and so allow the head to impact the ground.

Motion laws have been applied to joints for few instants, in order to reproduce a specific scenario and then letting the gravity act on the body.
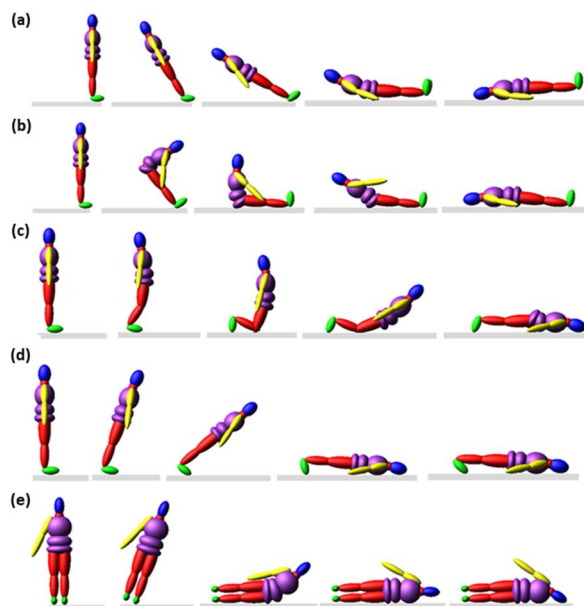
Fig. 5. (a) Scenario 1; (b) Scenario 2; (c) Scenario 3; (d) Scenario 4; (e) Scenario 5.

Table 6. Head peak force comparison between dummy model and numerical model.

	Peak Impact Force [kN]				
	Scenario 1	**Scenario 2**	**Scenario 3**	**Scenario 4**	**Scenario 5**
Experimental (Dummy)	22.8 ± 2.1	14.9 ± 4.6	20.3 ± 3.7	21.6 ± 6.1	17.1 ± 2.2
Simulation (Model)	22.9	14.83	21.46	24	18.6
Analytical Deviation	$\Delta = 0.1\ [kN]$ $\Delta\% = 0.44\%$	$\Delta = -0.07\ [kN]$ $\Delta\% = -0.47\%$	$\Delta = 1.16\ [kN]$ $\Delta\% = 5.7\%$	$\Delta = 2.4\ [kN]$ $\Delta\% = 11\%$	$\Delta = 1.5\ [kN]$ $\Delta\% = 8.8\%$

The model is able to properly simulate impact forces, being the experimental and numerical results very close to each other, as well as configurations at every time instant. These results have been obtained after a proper tuning of the model parameters, in order to make the android model as close as possible to the dummy. So, for example, in scenario 1 if both motions of the lumbar and thoracic joints are left free (inside their ROM), the peak force head's value is about 15 kN, because the upper torso impact becomes the most relevant. On the other side, if the upper torso is constrained to have zero rotations, the head peak force assumes the value reported in Table 6.

In addition, all force values are above the thresholds required to produce a fatal impact (Allsop et al., (1991); Hajiaghamemar et al., (2015); Yoganandan et al., (1995)).

A fall from a height has also been simulated; the model reproduces two different situations of an accidental fall from a height of about 3 m from the ground, where a geometry representing the floor was created as well as the surrounding environment, in order to evaluate android-environment interaction during the fall (Fig. 6).
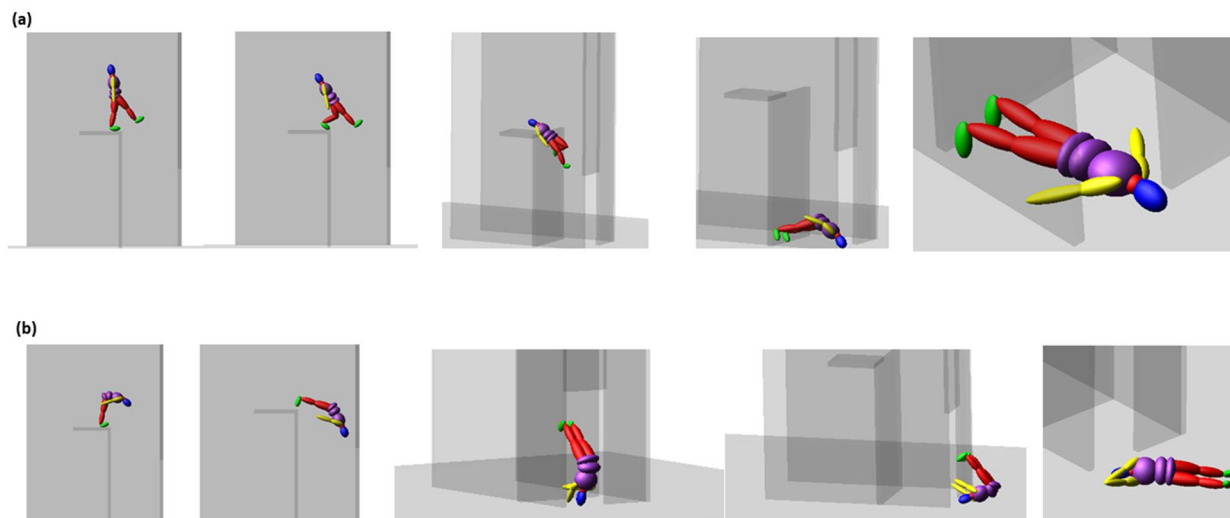
Fig. 6. (a) Accidental fall after a gait step; (b) Accidental fall for unbalanced starting configuration.

Segments and joints motions are realistic during the fall, when the android interacts with the environment and at the time of its impact with the ground; therefore, suitable resistive parameters have been assigned; also the contact sequence of body parts is logical, creating realistic final configurations.

4. Discussion

Body dimensions and inertial properties as well as joint centres have been obtained from anthropometric databases through regression, having given the subject height and weight as independent variables. This means that 'average' morphometric, inertial and kinematic properties have been used. If the individual is different from the 'average individual' corresponding to his height and weight, the adopted numerical model might not be truly representative. More accurate results could be obtained through a more accurate anthropometric study of the victim.

The present model does not include internal organs; therefore injuries cannot be studied in details, and it is confined to the study of body trajectories and of body interaction with the surrounding environment. The impossibility of simulating trauma and the respective energy absorption makes the multibody behave more elastically than in reality.

Other joints could be taken into account as well, but test performed by other authors demonstrated that the movement of end body parts (such as feet, hands and forearms) have a negligible influence (Milanowicz et al., (2017)); therefore this approach should provide a good approximation.

A further validation of results can be performed calculating the likelihood of injuries (through AIS that is the Abbreviated Injury Score) based on each body segment injury criteria ((Aldieri et al., (2018)), King, (2001), (2000); Prasad et al., (2010)), and comparing the outcome to findings from the medical autopsy.

On the whole, the analysis of falls from height requires a multidisciplinary approach where biomechanical models can provide some useful information. Other information should nonetheless be provided, for example by legal medicine which should contribute to establish the energy necessary to procure certain trauma and injuries in the victim (Zanetti et al., (2014)).

References

Aldieri, A., Terzini, M., Osella, G., Priola, A.M., Angeli, A., Veltri, A., Audenino, A.L., Bignardi, C., 2018. Osteoporotic Hip Fracture Prediction: Is T-Score-Based Criterion Enough? A Hip Structural Analysis-Based Model. Journal of Biomechanical Engineering 140.
Allsop, D.L., Perl, T.R., Warner, C.Y., 1991. Force/deflection and fracture characteristics of the temporo-parietal region of the human head. Proceedings - Society of Automotive Engineers 269–278.

Atanasijevic, T., Popovic, V., Mihailovic, Z., Radnic, B., Soldatovic, I., Nikolic, S., 2015. Analysis of Closed Soft Tissue Subcutaneous Injuries"Impact Décollement" in Fatal Free Falls From Height—Forensic Aspect. The American Journal of Forensic Medicine and Pathology 36, 145–148.

Bergmark, A., 1989. Stability of the Lumbar Spine: A Study, in "Mechanical Engineering, Acta orthopaedica Scandinavica: Supplementum". In: Munksgaard, Copenhagen, pp.54.

Cheng, H., Rizer, A.L., Obergefell, L.A., 1998. Articulated Total Body Model Version V; User's Manual.

Dong, X.S., Largay, J.A., Choi, S.D., Wang, X., Cain, C.T., Romano, N., 2017. Fatal falls and PFAS use in the construction industry: Findings from the NIOSH FACE reports. Accident Analysis and Prevention 102, 136–143.

Engin, A.E., 1979. Measurement of resistive torques in major human joints.

Engin, A.E., Chen, S., 1987. Kinematic and Passive Resistive Properties of Human Elbow Complex

Farina, E., Bianco, S., Bena, A., Pasqualini, O., 2019. Finding causation in occupational fatalities: A latent class analysis . American Journal of Industrial Medicine 62, 123–130.

Hajiaghamemar, M., Seidi, M., Ferguson, J.R., Caccese, V., 2015. Measurement of Head Impact Due to Standing Fall in Adults Using Anthropomorphic Test Dummies. Annals of Biomedical Engineering 43, 2143–2152.

Haug, E., Robin, S., Beaugonin, M., 2004. Human Models for Crash and Impact Simulation, in "Computational Models for the Human BodySpecial Volume of Handbook Of Numerical Analysis" . In: Ayache, N. (Ed.). P.G. Ciarlet, Houston, pp. 676

King, A.I., 2000. Fundamentals of Impact Biomechanics: Part I - Biomechanics of the Head, Neck, and Thorax Annual Review of Biomedical Engineering 2, 55–81.

King, A.I., 2001. Fundamentals Of Impact Biomechanics: Part 2—Biomechanics of the Abdomen, Pelvis, and Lower Extremities. Annual Review of Biomedical Engineering 3, 27–55.

Milanowicz, M., Kędzior, K., 2017. Active numerical model of human body for reconstruction of falls from height. Forensic Science International 270, 223–231.

Muggenthaler, H., Drobnik, S., Hubig, M., Schönpflug, M., Mall, G., 2013. Fall from a Balcony-Accidental or Homicidal? Reconstruction by Numerical Simulation. Journal of Forensic Science 58, 1061–1064.

Pascoletti, G., Cianetti, F., Putame, G., Terzini, M., Zanetti, E.M., 2018. Numerical Simulation of an Intramedullary Elastic Nail: Expansion Phase and Load-Bearing Behavior. Frontiers in Bioengineering and Biotechnology 6.

Prasad, P., Mertz, H.J., Dalmotas, D.J., Augenstein, J.S., Diggs, K., 2010. Evaluation of the field relevance of several injury risk functions. Stapp Car Crash Journal 54, 49–72.

Putame, G., Terzini, M., Bignardi, C., Beale, B., Hulse, D., Zanetti, E., Audenino, A., 2019. Surgical Treatments for Canine Anterior Cruciate Ligament Rupture: Assessing Functional Recovery Through Multibody Comparative Analysis. Frontiers in Bioengineering and Biotechnology 7, 180.

Riener, R., Edrich, T., 1999. Identification of passive elastic joint moments in the lower extremities. Journal og Biomechanics 32, 539–544.

Robbins, D.H., 1983. Anthropometric specifications for mid-sized male dummy, volume 2, and for small female and large male dummies, volume 3. Final report.

Rowbotham, S.K., Blau, S., 2016. Skeletal fractures resulting from fatal falls: A review of the literature Forensic Science International 266, 582.e1--582.e15.

Rowbotham, S.K., Blau, S., Hislop-Jambrich, J., Francis, V., 2018. Skeletal Trauma Resulting From Fatal Low (≤3 m) Free Falls: An Analysis of Fracture Patterns and Morphologies Jpurnal of Forensic Science 63, 1010–1020.

Sharan, A.D., Tang, S.Y., Vaccaro, A.R., 2013. Basic Science of Spinal Diseases. In: Jaypee Brothers,Medical Publishers Pvt. Limited, London, pp. 300.

Terzini, M., Zanetti, E.M., Audenino, A.L., Putame, G., Gastaldi, L., Pastorelli, S., Panero, E., Sard, A., Bignardi, C., 2017. Multibody modelling of ligamentous and bony stabilizers in the human elbow. Muscles, ligaments and tendons journal 7, 493–502.

Yoganandan, N., Pintar, F.A., Sances, A., Walsh, P.R., Ewing, C.L., Thomas, D.J., Snyder, R.G., 1995. Biomechanics of Skull Fracture. Journal of Neurotrauma 12, 659–668.

Zanetti, E.M., Franceschini, G., Audenino, A.L., 2014. Rider–handlebar injury in two-wheel frontal collisions. Joutnal of Mechanical Behavior of Biomedical Materials 33, 84–92.

Zanetti, E., Terzini, M., Mossa, L., Bignardi, C., Costa, P., Audenino, A., Vezzoni, A., 2017. A structural numerical model for the optimization of double pelvic osteotomy in the early treatment of canine hip dysplasia. Veterinary and Comparative Orthopaedics and Traumatology 30, 256–264.

Zanetti, E.M., Bignardi, C., Terzini, M., Putame, G., Audenino, A.L., 2018. A multibody model for the optimization of hip arthroplasty in relation to range of movement. Australasian Medical Journal 11, 486–491.